THE DETAILED OPTICAL DESIGN OF A DOUBLE-PASS LITTROW MONOCHROMATOR FOR A MARS ATMOSPHERIC WATER DETECTION SPECTROPHOTOMETER

By: B. D. Henderson

FINAL REPORT

Contract No. 952552

Prepared for:

California Institute of Technology
Jet Propulsion Laboratory

FR-2579-101

THE DETAILED OPTICAL DESIGN
OF A DOUBLE-PASS LITTROW MONOCHROMATOR
FOR A
MARS ATMOSPHERIC WATER DETECTION SPECTROPHOTOMETER

By: B. D. Henderson

FINAL REPORT

AUG 1969

Contract No. 952552

This work was performed for the Jet Propulsion Laboratory, California Institute of Technology, sponsored by the National Aeronautics and Space Administration under Contract NAS7-100.

Prepared for

California Institute of Technology
Jet Propulsion Laboratory

Beckman® INSTRUMENTS, INC.
ADVANCED TECHNOLOGY OPERATIONS
FULLERTON, CALIFORNIA • 92634

TABLE OF CONTENTS

LIST OF ILLUSTRATIONS

1.0 INTRODUCTION

This is the second and final report prepared for the Jet Propulsion Laboratory under Contract No. 952552 for the development of a design--using ray-trace analysis--for a Mars Atmospheric Water Detection Spectrophotometer. The preliminary report presented a comparative analysis of nine monochromator configurations, each of which was physically no longer than fifty percent of its effective dispersive focal length. This is an important requirement for this spectrophotometer, since its dispersive focal length must be nearly 1000 mm, yet the instrument structure not be much over 500 mm in length.

The nine monochromator configurations were made up of one single-pass monochromator with a Cassegrainian collimating system and eight double-pass monochromators. These monochromators consisted of both Ebert and Littrow types having all combinations of either a spherical or paraboloid collimating mirror, with either a corner mirror or corner prism used as the return reflector at the intermediate spectral image.

Of these nine monochromator configurations, only three--the Cassegrainian monochromator and the double-pass Littrow monochromators using a paraboloid collimating mirror with either a corner mirror or corner prism--gave sufficiently good spectral image quality for its application. These three monochromator configurations have spectral image aberrations which are smaller than 10 percent of the spectral bandwidth which was specified for the four frequencies used in the preliminary study.

The preliminary report was a comparative mathematical analysis of any monochromator optical configuration which appeared feasible for this application. This final report, on the other hand, is more of an optical engineering report which presents a critical analysis of only one preferred monochromator configuration.

The resultant physical locations of the optical elements in the final monochromator design are compromises which optimize both physical mounting considerations and spectral image quality.

JPL has selected the double-pass Littrow monochromator which uses a paraboloid collimating mirror and a return prism for the final spectrophotometer design, as a result of the investigation presented in the preliminary report. The choice of a double-pass monochromator over the Cassegrainian monochromator is based primarily on the fact that the Cassegrainian system requires both the grating and the collimating mirror to be twice as large in linear dimensions and nearly eight times more massive than those required by the double-pass monochromator. Although the double-pass monochromator may be a little longer than the Cassegrainian monochromator, the structural cross sectional area of the double-pass monochromator will be four times smaller. The return prism has been selected--rather than the return mirrors--since high accuracy prisms are much easier to manufacture, mount, and service than high-accuracy, double-mirror systems.

The best locations for each optical surface in the final monochromator design are controlled by several factors:

a. Providing for the large volume occupied by the grating and its supporting surfaces;

b. Supporting the PbS detectors and the entrance slit on a common substrate with a fused-silica cover plate ov the detectors;

c. Providing the proper entrance slit curvature on the substrate and providing the substrate with the proper tilt forward to optimize the spectral image flatness for all the PbS detectors.

JPL has specified five new frequencies for the final monochromator design instead of the four frequencies used in the preliminary report. JPL has further requested Beckman to investigate available line emission sources to determine whether one can be used as a frequency calibration source. Such a source must have one or more strong emission lines within, or near to, the five frequencies which have been specified. It is, of course, suitable to use the 2nd, 3rd, or 4th orders of an emission line frequency.

The physical dimensions of the final monochromator design that are described in this report are nearly the same as those dimensions used for the double-pass Littrow monochromator which had a paraboloid collimating mirror and a return prism and which was analyzed in the preliminary report. There are these differences:

a. The grating ruled surface has been moved 75 mm in front of the entrance slit to obtain sufficient mechanical clearance for the entrance slit and PbS detector assembly, the return prism, and a mechanical chopper to be mounted in front of the prism.

b. A 0.25-mm-thick fused-silica plate has been placed in the optical path in front of PbS detectors. The detectors are cemented to the back face of this plate.

c. The entrance slit is mounted to and flush with the front face of the same fused-silica plate. An opening is provided through the plate directly behind the entrance slit so the light rays passing through the entrance slit do not interfere with the plate.

d. The entrance slit is no longer straight and parallel to the grooves of the grating, but is slightly curved and tilted. However, it is still flush with the front face of the fused-silica plate. This new entrance slit spacial orientation produces spectral images that are perfectly straight and parallel at each of the PbS detectors. The fused-silica plate is further tipped 0.8° from the vertical to bring all of the PbS detectors to an optimal focus.

The spectral image quality of the final monochromator design has been found to be very good. The maximum aberration spread for each of the five frequencies is less than ten percent of the PbS detector widths. The three center frequencies--which are the most important analytically--have aberration spreads that are less than five percent of the PbS detector widths.

A search for a calibration source has shown that a Kryton arc produces a relatively strong and well isolated emission line at 6904.68 Å, which has a second order spectral image 1.6 mm from the entrance slit. This image, furthermore, is on the opposite side of the entrance slit from the images of the five frequencies.
This Kryton emission line may be straddled by two PbS detectors which are mounted to the same substrate as the entrance slit and the other five PbS detectors. Any wavelength error in the monochromator during operation will cause a lateral shift of the spectral image of the Kryton emission line relative to these two detectors.

2.0 FINAL PERFORMANCE REQUIREMENTS

JPL has modified several of the performance requirements outlined in the Preliminary Report, and these modifications have been included in this final monochromator design. The final performance requirements for the Mars Atmospheric Water Detection Spectrophotometer are now as follows:

a. The monochromator shall have a 1000-mm focal length and a f/5 relative square aperture.

b. The grating shall have 1200 line/mm with a blaze at 1.2μ, and a blaze angle of 46° 4'.

c. The entrance slit is to be 0.25 mm wide by 3.5 mm high.

d. The PbS detectors shall be located on the spectral image surface to solely define the frequency bandpasses. The PbS detectors are to have sensitive areas 0.25-mm wide in the direction of dispersion by 1.0 mm high. They are to be mounted on a common substrate and protected with a 0.25-mm-thick, fused-silica plate which is cemented to their sensitive surfaces.

e. The center frequencies to be detected are:

   1. 7229.09 cm^{-1}
   2. 7230.90 cm^{-1}
   3. 7232.12 cm^{-1}
   4. 7234.85 cm^{-1}
   5. 7236.27 cm^{-1}

f. The frequency resolution at the PbS detectors must be at least 1 cm^{-1}, and preferably 0.65 cm^{-1}.

g. The second order of the 6904.68Å Kryton line is to be used for frequency calibration. Its spectral image is to be straddled by the two PbS detectors.

3.0 DESCRIPTION OF THE MONOCHROMATOR

A schematic diagram of the final monochromator design is shown in Figure 1, and it is rigorously defined by Tables I, II, and III. In operation, light rays travel successively from the entrance slit of the monochromator--which is in the (X_o, Y_o, Z_o) axis system--to the collimating mirror, grating, collimating mirror, return prism, collimating mirror, grating, collimating mirror, and finally the spectral image surface--which is in the (X_{16}, Y_{16}, Z_{16}) axis system. The entrance slit and the PbS detectors which are each at a spectral image of the entrance slit have only positive Y-values in their respective axis systems. The first spectral image which is formed of the entrance slit is formed with approximately unity magnification in the return prism and it has all negative Y values. The second spectral image of the entrance slit is formed on the PbS detectors.

To obtain the best overall spectral image quality for the five analytical frequencies, and for the Kryton calibration frequency, the entrance slit has been offset along the positive Z_o axis as shown in the upper chart of Table IV. Five entrance slit starting points are used for the ray trace, and their Z_o values range from 1.0 mm to 0.846 mm; therefore, the best image quality is obtained in the vicinity of Z_{16} = -0.9 mm. The five analytical frequencies are approximately centered about Z_{16} = -0.9 mm.

The single collimating mirror of this monochromator is a paraboloid of 500 mm focal length. Since the light rays travel through the monochromator twice in succession, the spectral dispersion of the entrance slit image at the PbS detectors is equivalent to that formed by a single monochromator having a 1000-mm focal length.

The diffraction grating is a replica grating of 1200 line/mm. It is used in the first order for the five analytical frequencies and in the second order for the

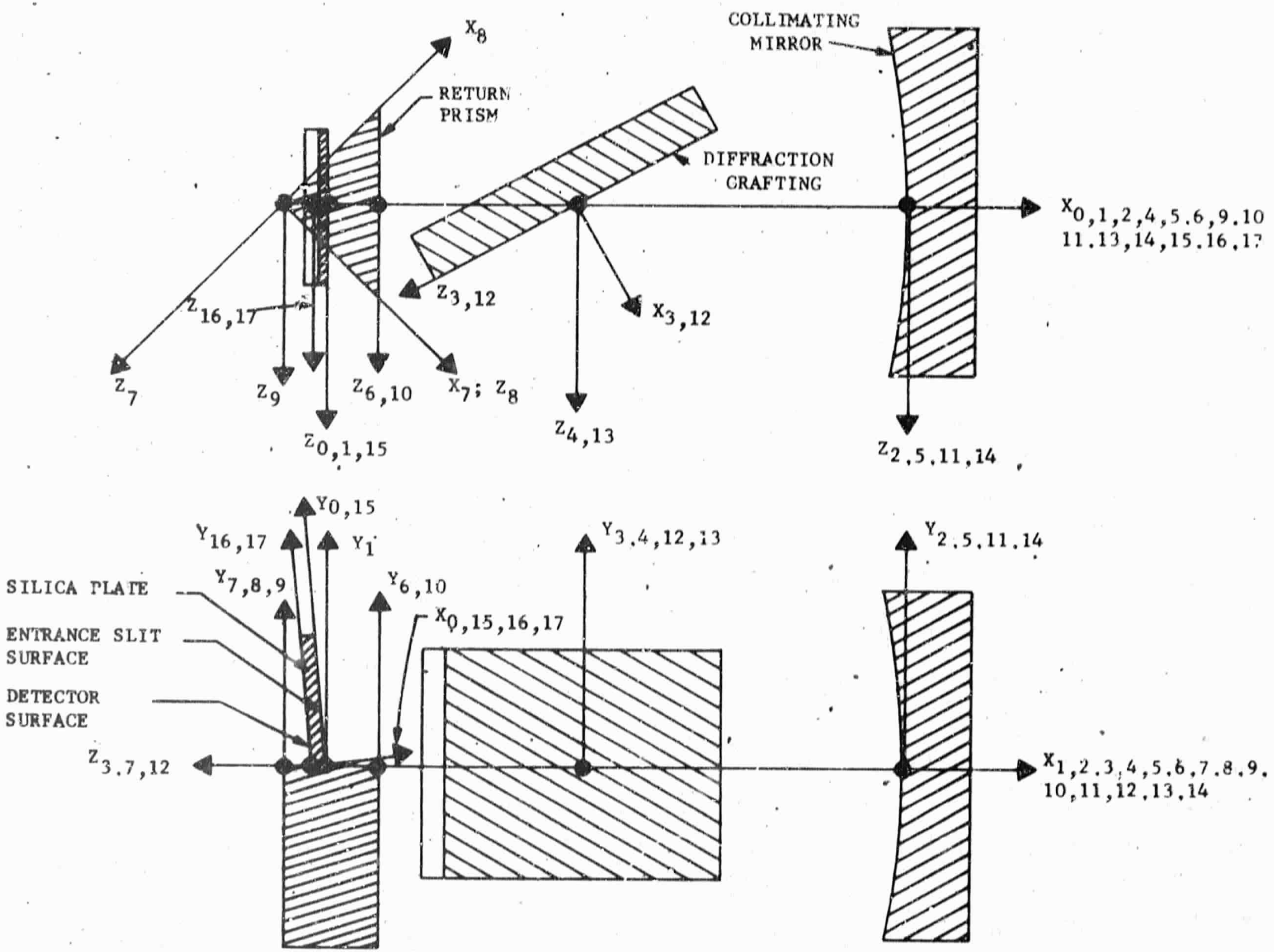

Figure 1. Optical Schematic

Table I (Sheet 1 of 2). Definition of Axis Systems for the Double-Pass Littrow Monochromator with a Return Prism.

(X_o, Y_o, Z_o)	ENTRANCE SLIT--The entrance slit is on the $Y_o - Z_o$ plane.
(X_1, Y_1, Z_1)	MATHEMATICAL AXIS SYSTEM--This axis system has the same origin as the (X_o, Y_o, Z_o) and (X_{15}, Y_{15}, Z_{15}) axis systems, and it is used only as a mathematical aid.
(X_2, Y_2, Z_2) (X_5, Y_5, Z_5) (X_{11}, Y_{11}, Z_{11}) (X_{14}, Y_{14}, Z_{14})	COLLIMATING MIRROR--These four axis systems are identical. The collimating mirror is tangential to the $Y_{2,5,11,14}-Z_{2,5,11,14}$ plane at the origin. The focus of this paraboloid collimating mirror is located on the negative $X_{2,5,11,14}$ axis.
(X_3, Y_3, Z_3) (X_{12}, Y_{12}, Z_{12})	DIFFRACTION GRATING--These two axis systems are identical. The grating surface is on the $Y_{3,12} - Z_{3,12}$ plane, and the grating rulings are parallel to the $Y_{3,12}$ axis.
(X_4, Y_4, Z_4) (X_{13}, Y_{13}, Z_{13})	MATHEMATICAL AXIS SYSTEMS--These two axis systems are identical. They have the same origin as the $(X_{3,12}, Y_{3,12}, Z_{3,12})$ axis system, and they are used only as a mathematical aid.
(X_6, Y_6, Z_6) (X_7, Y_7, Z_7) (X_8, Y_8, Z_8) (X_{10}, Y_{10}, Z_{10})	RETURN PRISM--The $Y_{6,10} - Z_{6,10}$ plane is used as the transmitting face of the prism, and the $Y_7 - Z_7$ and $Y_8 - Z_8$ planes are the internal reflecting faces. The Y_7, Y_8, and Y_9 axes are identical and parallel to the $Y_{6,10}$ axis. The Z_7 axis is at 90° to the Z_8 axis and the $Z_{6,10}$ axis is at 45° to both the Z_7 axis and the Z_8 axis.

Table I (Sheet 2 of 2). Definition of Axis Systems for the Double-Pass Littrow Monochromator with a Return Prism.

(X_9, Y_9, Z_9)	MATHEMATICAL AXIS SYSTEM--This axis system has the same origin as the (X_7, Y_7, Z_7) and (X_8, Y_8, Z_8) axis systems, and it is used only as a mathematical aid.
(X_{15}, Y_{15}, Z_{15})	FRONT FACE OF DETECTOR COVER PLATE--A 0.25-mm-thick quartz plate covers the photo-detectors for protection. The front face of this plate is on the $Y_{15} - Z_{15}$ plane. This axis system is identical to the (X_o, Y_o, Z_o) axis system.
(X_{16}, Y_{16}, Z_{16})	BACK FACE OF DETECTOR COVER PLATE--The photodetectors are mounted on the $Y_{16} - Z_{16}$ plane at the spectral images of each required frequency.
(X_{17}, Y_{17}, Z_{17})	SPECTRAL IMAGE FOCUSING SURFACE--This axis system is used only when the computer automatic focusing program is used. This axis system is set identical to the (X_{16}, Y_{16}, Z_{16}) axis system at the start of each ray trace. The computer then moves this axis system along the X_{16} axis by mathematical iteration until the ray-traced image on the $Y_{17} - Z_{17}$ plane has a least square deviation.

Table II. Definitions of Dimensional Parameters Used in Table III

A_n -- The X_{n-1} coordinate for the origin of the (X_n, Y_n, Z_n) axis system measured in the $(X_{n-1}, Y_{n-1}, Z_{n-1})$ axis system.

B_n -- The Y_{n-1} coordinate for the origin of the (X_n, Y_n, Z_n) axis system measured in the $(X_{n-1}, Y_{n-1}, Z_{n-1})$ axis system.

C_n -- The Z_{n-1} coordinate for the origin of the (X_n, Y_n, Z_n) axis system measured in the $(X_{n-1}, Y_{n-1}, Z_{n-1})$ axis system.

α_n -- The Angular displacement of the X_n axis from the X_{n-1} axis measured in the X_{n-1}-Z_{n-1} plane. This angle is positive when the X_n axis is moved toward the positive Z_{n-1} axis, and negative when moved toward the negative Z_{n-1} axis.

β_n -- The angular displacement of the X_n axis from the X_{n-1} axis measured in the X_{n-1}-Y_{n-1} plane. This angle is positive when the X_n axis is moved toward the positive Y_{n-1} axis, and negative when moved toward the negative Y_{n-1} axis.

γ_n -- The angular displacement of the Z_n axis from the Z_{n-1} axis measured in the Y_{n-1}-Z_{n-1} plane. This angle is positive when the Z_n axis is moved toward the positive Y_{n-1} axis, and negative when moved toward the negative Y_{n-1} axis.

Table III. Dimensions of the Final Monochromator Optical System

AXIS SUBSCRIPT	A	B	C	α	β	γ
1	0	0	0	0	-0.8	0
2	500.0	0	0	0	0	0
3	-425.0	0	0	56.055	0	0
4	0	0	0	-56.055	0	0
5	425.0	0	0	0	0	0
6	-496.4416	0	0	0	0	0
7	-5.0	0	0	45.0	0	0
8	0	0	0	-90.0	0	0
9	0	0	0	45.0	0	0
10	5.0	0	0	0	0	0
11	496.4416	0	0	0	0	0
12	-425.0	0	0	56.055	0	0
13	0	0	0	-56.055	0	0
14	425.0	0	0	0	0	0
15	-500.0	0	0	0	0.8	0
16	-0.25	0	0	0	0	0
17	0	0	0	0	0	0

A, B, C in mm

α, β, γ in degrees

Table IV. Ray-Defining Coordinates for the Final Monochromator Optical System

Points	X_o	Y_o	Z_o
1	0	2.0	1.0
2	0	2.5	0.987
3	0	3.75	0.942
4	0	5.0	0.877
5	0	5.5	0.846

The five Entrance Slit Starting Points

Corner	X_3	Y_3	Z_3
1	0	50.0	-90.0
2	0	50.0	90.0
3	0	-50.0	90.0
4	0	-50.0	-90.0

The Four Corner Points of the Grating Used Area Which Define the Field Stop of the Monochromator

Kryton calibration frequency. The grating is blazed at 1.2μ, which insures a good grating efficiency at all the six frequencies involved.

The grating must be provided with a hole cut through its center to transfer light rays between the collimating mirror and the entrance slit, return prism, and PbS detectors. This hole is preferably cut in the grating substrate before the grating replication is performed. The ruled area of the grating is 100 mm measured along the grooves and 180 mm measured across the grooves. The grating is mounted with the grating normal rotated 56.055° from the optical axis. The grating ruled area for the first pass of the monochromator has been defined as the aperture stop for the monochromator. The lower chart of Table IV gives the coordinates of the ruled area of the grating in the (X_3, Y_3, Z_3) axis system. These same coordinates define the monochromator aperture stop for every ray trace. The grating ruled area subtends a 100-mm square area measured normal to the optical axis; thus, the monochromator has a relative square aperture of f/5.

The return prism is a 45°-90°-45° solid prism made from fused silica. The widths of the three faces are approximately 7.07 mm x 10.00 mm x 7.07 mm. The prism can be made as long as necessary (measured normal to the prismatic cross section) to aid in supporting the prism from surfaces that are well away from the prism's used surfaces. The top end of the prism should be at the optical axis. All portions of the prism will then have negative Y-locations. This will insure that the prism does not interfere with light rays traveling from the entrance slit and to the PbS detectors.

The entrance slit and the PbS detectors are in physical contact with a 0.25-mm thick, fused-silica plate. The entrance slit is considered to be a photo-etched slot in a thin metal sheet which lies flat on the front surface of the fused silica plate. An opening will be drilled through the plate immediately behind the slit to allow the incident light rays to pass through the entrance slit without interference by the plate. The PbS detectors are flush with the back surface of the fused silica plate except for a thin film of cement which holds the two together. The photo-deposited detectors can be rectangular, 0.25-mm wide x 1 mm high, and their locations are completely determined by the ray trace analysis reported here.

4.0 RAY TRACE PROCEDURES

The optimization of the monochromator optical design was accomplished by several ray-trace iterations varying several monochromator parameters listed in Tables III and IV, namely β_1 and β_{15}; A_6 and A_{11}; and Z_o. Each ray-trace analysis was used to determine the optical performance characteristics of the monochromator after each modification of parameters.

The ray-trace program that has been applied utilizes a separate three-dimensional axis system for each optical surface, or for each plane that is used to analyze for image quality. This final monochromator design requires sixteen axis systems to define all of its optical surfaces. A seventeen-axis system is used to measure the distance from the sixteen-axis system to the best focus for all combinations of each frequency and each entrance slit starting point.

In performing each ray trace analysis of the monochromator, the same type of ray family has been used for each frequency and for each of the five starting points on the entrance slit. A ray family is defined here as a group of rays that start from a single point on the entrance slit, and upon the first encounter with the grating surface, the group of rays spreads out so as to intersect the grating surface in a uniform array of intersection points which consists of an equal number of columns and rows of points. The boundaries of the array for each ray family precisely matches the ruled area of the grating. This makes the ruled area of the grating the aperture stop of the monochromator optical system.

A family of rays may consist typically of 4, 9, 81, or 100 rays. A four-ray family is generally sufficient to define the physical boundaries of the optically-used areas at each optical surface in the monochromator system. That is, of course, because these four rays intersect the four corners of the aperture stop. A nine-ray family not only can define the physical boundary conditions, but it has one ray which is the centroid of its array. Furthermore, it has a sufficient number of rays to give a usable knowledge about the nature of the optical aberrations at the spectral images of its starting point. An eighty-one ray family also provides one ray at the centroid of its array, and it has sufficient rays to analyze the characteristics of image aberrations in fine detail. A one-hundred-ray family does not have a centroid ray, but it is convenient for analyzing image characteristics as a percent of a total image array, since each ray accounts for one percent of the array.

5.0 SPECTRAL IMAGE ANALYSIS

This analysis consisted of finding the spectral image location and aberration content for thirty separate families of rays representing all combinations of five entrance-slit starting points and six center frequencies (five analytical frequencies and one Kryton calibration frequency). Each of the thirty family of rays consisted of one hundred rays. The best focus for each one-hundred-ray family was computed on the Y_{17}-Z_{17} plane which was automatically translated along the X_{16}-axis by the computer until a least-square aberration existed as measured in the direction of dispersion (along the Z_{17}-axis).

The A_{17} values (movement of the Y_{17}-Z_{17} plane along the X_{16}-axis) for the thirty ray family then describe the shape of the true monochromator focal surface relative to the (X_{16}, Y_{16}, Z_{16}) axis system. Once the computer has determined the true focal position for a family of rays, it then also calculates the centroid, the total image spread for all 100 rays, the best 99 rays, the best 98 rays, the best 95 rays, the best 90 rays, and the best 75 rays, as measured in the direction of dispersion. Further, the ray density for small aberration intervals measured in the direction of dispersion are tabulated by the computer for each family.

Several ray trace trials were required in which β_1, β_{15}, A_6, A_{11}, and Z_o were changed slightly. For the first trial β_1 and β_{15} were equal to zero and Z_o was equal to 1.0 mm for Y_o = 2.0, 2.5, 3.75, 5.0, and 5.5 The monochromator focal surface was not parallel to the Y_{16}-Z_{16} plane on which the PbS detectors are in contact, and the spectral images of the five entrance slit starting points were neither in a straight line nor parallel to the Y_{16}-axis. For the final monochromator design, the five entrance slit starting points shown in the upper chart of Table IV are displaced from parallelism with the Y_o-axis and are also curved sufficiently to make all six of the spectral images of the entrance slit straight and parallel to the Y_{16}-axis. The fused-silica plate was also rotated through 0.8° around a fixed $Z_{0,15}$-axis, to obtain the best monochromator focal surface match with the Y_{16}-Z_{16} plane for all thirty spectral images.

Figure 2 is a composite graph of the locations of the five entrance slit starting points on the Y_0-Z_0 plane, and the locations of their thirty spectral images on the Y_{16}-Z_{16} plane as viewed from inside the monochromator looking parallel to the $X_{0,16}$-axis. The Y_0-Z_0 plane is 0.25 mm in front of the Y_{16}-Z_{16} plane as separated by the fused silica plate. The Z_0-value is printed at each of the entrance slit starting points. Two numbers are printed at each of the thirty spectral images. The upper number gives the distance of the best focus from the Y_{16}-Z_{16} plane. The positive values are in front of and negative values are behind the Y_{16}-Z_{16} plane. The lower numbers, which are in parenthesis, give the total aberration spread measured on the Z_{17}-axis for all 100 rays of each ray family. The Z_{16}-locations of each of the six spectral images is printed along each image. It is seen from Figure 2 that:

a. The spectral images are straight and parallel to the Y_{16}-axis. The computer output has shown that the centroids of each of the five points making up each of the six spectral images are parallel to the Y_{16}-axis within 0.001 mm, because of the entrance slit shape.

b. The focal surface for all the six frequencies is within ±0.030 mm of the PbS detector surfaces, which is the Y_{16}-Z_{16} plane. For the two preferred frequencies for the water analysis--7232.12 cm^{-1} and 7234.85 cm^{-1}--the focal surface deviates from Y_{16}-Z_{16} plane by less than +0.018 mm.

c. The total aberration spreads for the five analytical frequencies measured in the direction of dispersion are everywhere less than 0.025 mm, or 10 percent of the PbS detector width. For the two preferred frequencies--7232.12 cm^{-1} and 7234.85 cm^{-1}--the total aberration spread is less than 0.016 mm. The aberration spread for the Krypton line is less than 0.043 mm, or about 15 percent of the PbS detector width.

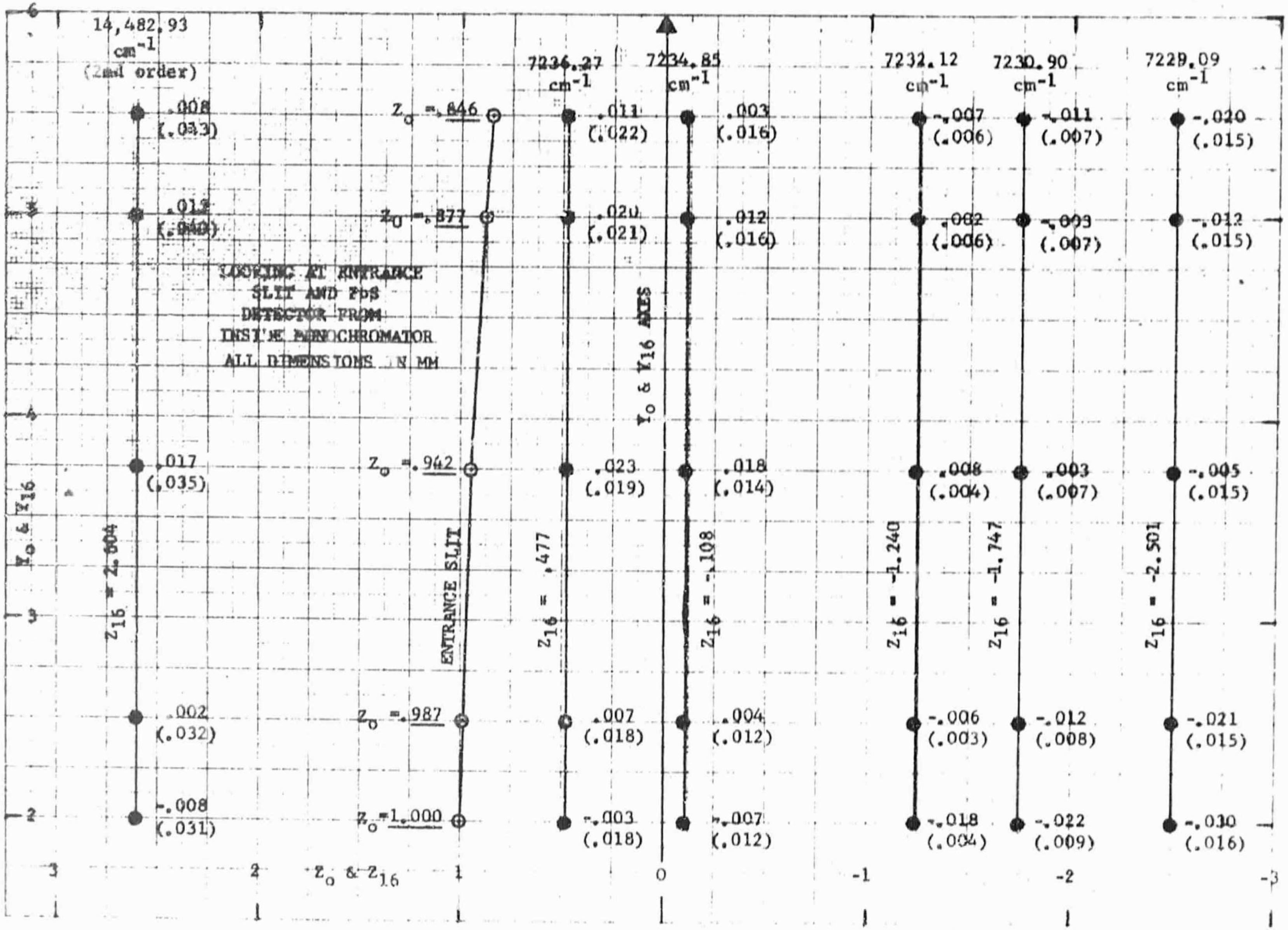

Figure 2. Spectral Image Characteristics

6.0 USED AREAS OF OPTICAL ELEMENTS

The ray-trace program computes and prints out the coordinates of the intersection of each ray with each optical surface in the axis system of that surface. It also prints out the direction cosines of each ray as it leaves a surface in the axis system of that surface. Since the printout of this much information for 100 ray families becomes expensive and cumbersome, it was not done for the 100-ray spectral image analysis.

For this final monochromator design, 4-ray families are sufficient to define the used areas of each optical element. Such 4-ray, ray traces were performed for the five analytical frequencies and the Kryton calibration frequency using only two entrance slit starting points: $Y_0 = 2.0$, and $Y_0 = 5.5$.

Figure 3 is a composite graph of the optical utilization of five different optical surfaces:

a. The entrance slit on the Y_0-Z_0 plane;

b. The six spectral images of the entrance slit on the Y_{16}-Z_{16} plane;

c. The transmitting face of the return prism on the $Y_{6,10}$-$Z_{6,10}$ plane;

d. The first internal reflecting surface in the return prism on the Y_7-Z_7 plane;

e. The second internal reflecting surface in the return prism on the Y_8-Z_8 plane.

This is a view from inside the monochromator looking parallel with the optical axis. All measurements are in mm. As in Figure 2, the entrance slit plane, Y_0-Z_0, is 0.25 mm in front of the PbS detector surfaces which are on the Y_{16}-Z_{16}

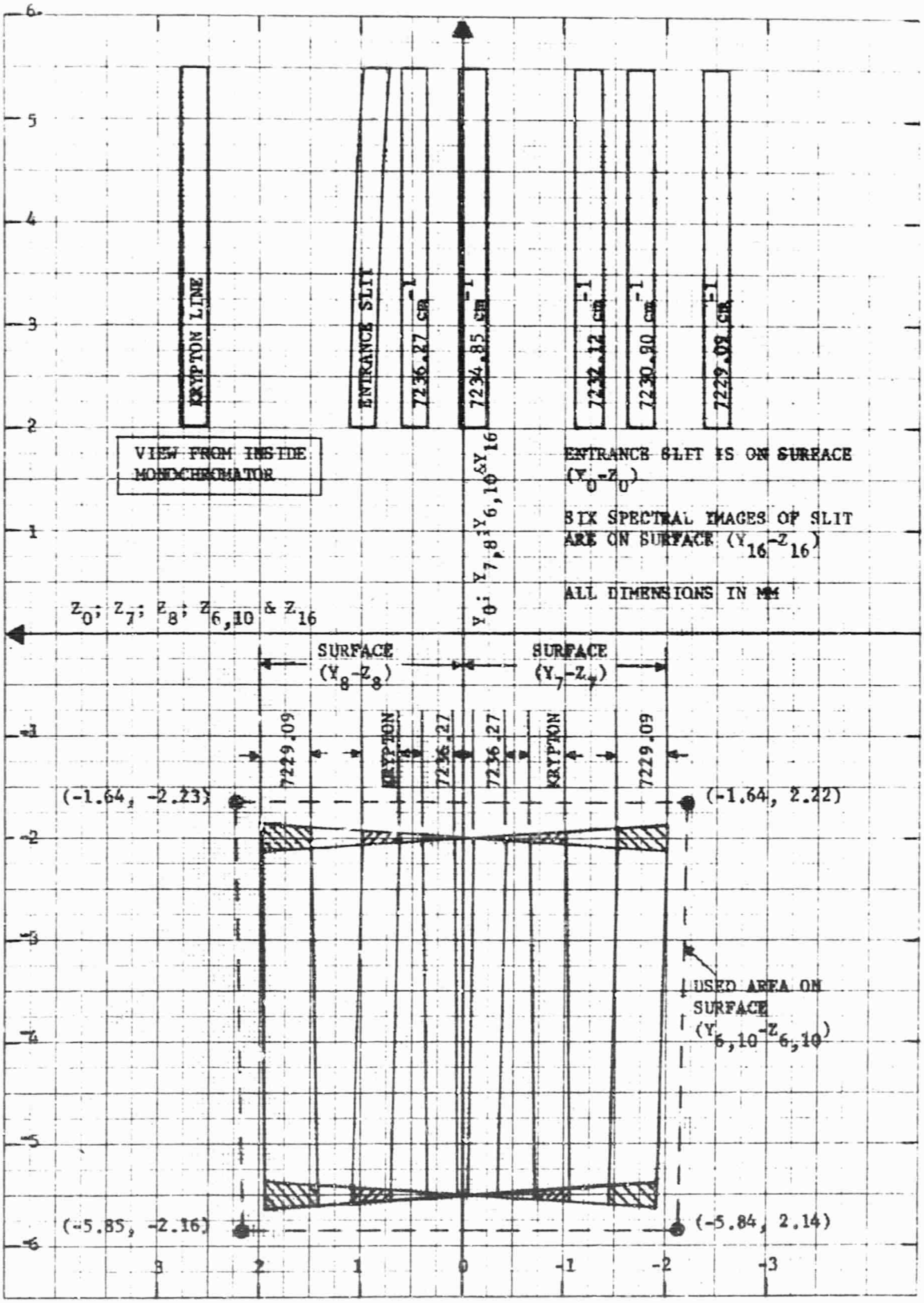

Figure 3. Optical Used Areas of Return Prism

plane, the 0.25-mm spacing being the fused-silica protective plate for the detectors. The width of the entrance slit and its six spectral images are shown as 0.25 mm.

Dashed lines surround the maximum area of use on the transmitting face of the return prism, which is the $Y_{6,10}-Z_{6,10}$ plane. The coordinates of the four corners of this used area are given. The actual edges of the return prism are at $Z_{6,10} = \pm 5.0$ mm, which are just off the edges of this graph on each side.

The locations of the 7229.09 cm^{-1}, 7236.27 cm^{-1}, and the Krypton images of the entrance slit are shown on the Y_7-Z_7 and Y_8-Z_8 planes, which are the internal reflecting surfaces of the return prism. The cross-hatched areas show the used areas for single horizontal lines 0.25 mm wide at $Y_0 = 2.0$, and $Y_0 = 5.5$ on the entrance slit. The 7236.27 cm^{-1} frequency images come nearest the corner of the prism which is the $Y_{7,8}$-axis, but do not actually cross into it. The used areas for the other three analytical frequencies are not shown in Figure 3, but they have image locations between the 7229.09 cm^{-1} and 7236.27 cm^{-1} locations.

Figure 4 is a graph of the used area of the collimating mirror. The coordinates of the four corner prints are given in mm.

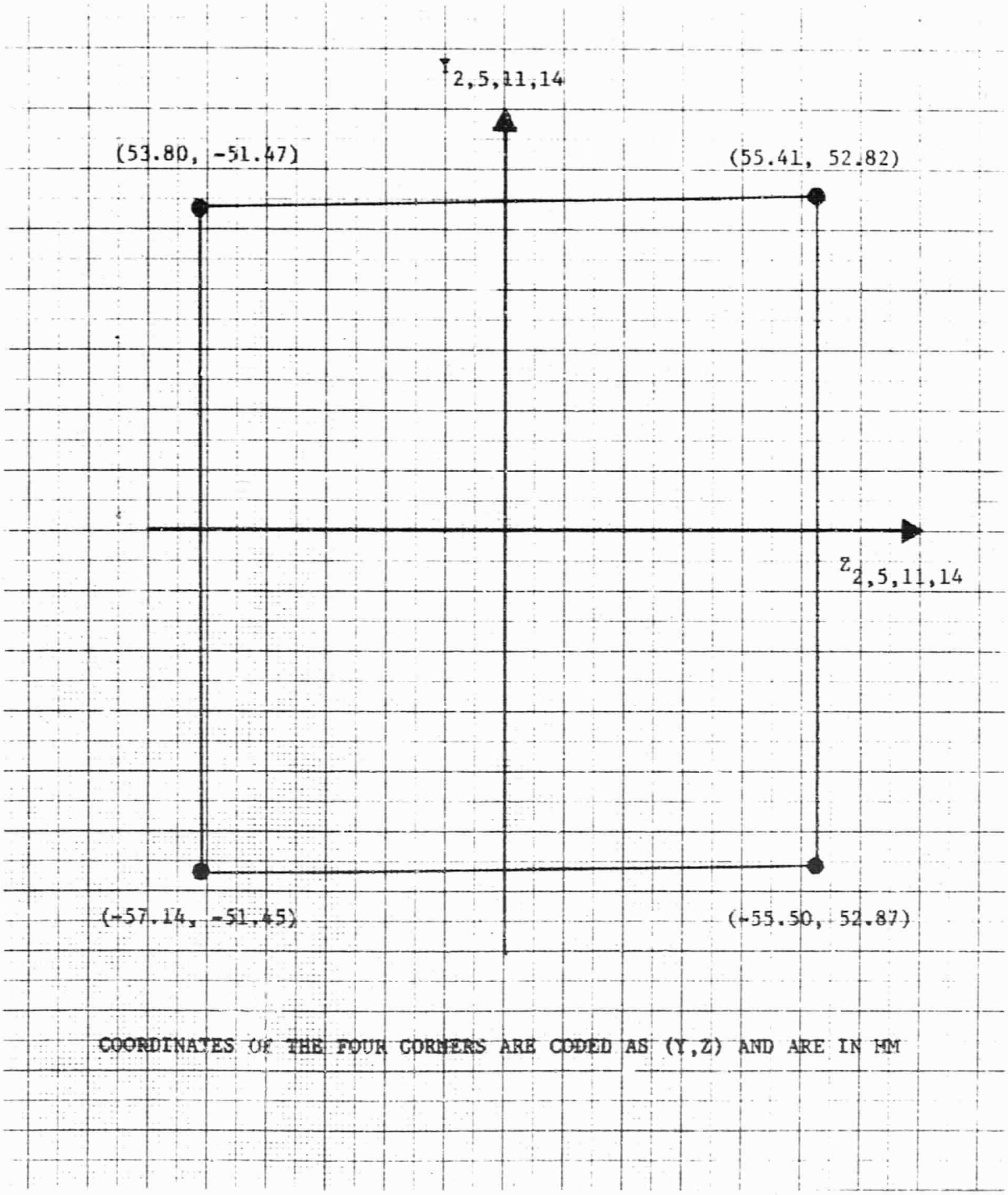

Figure 4. Optical Used Areas of Collimating Mirror

7.0 CONCLUSIONS

This report has described the optimization of a monochromator optical design using ray-trace techniques. It has shown that by the proper location and shape for the entrance slit, and by the proper locations for each of the photodetectors, the best possible image quality is obtained. This means that this monochromator design will give the best possible resolution for this application.